NASA TECHNICAL MEMORANDUM

NASA TM X- 71891

NASA TM X- 71891

RESULTS AND PROGRESS ON THE NASA LEWIS H_2-O_2 MHD PROGRAM

by J. Marlin Smith
Lewis Research Center
Cleveland, Ohio 44135

TECHNICAL PAPER to be presented at Fifteenth Symposium on the Engineering Aspects of Magnetohydrodynamics Philadelphia, Pennsylvania, May 24-26, 1976

RESULTS AND PROGRESS ON THE NASA LEWIS H_2-O_2 MHD PROGRAM

J. Marlin Smith
NASA Lewis Research Center
Cleveland, Ohio 44135

I. Introduction

The advantages, disadvantages, and possible applications of H_2-O_2 combustion driven MHD power generators have been discussed previously (refs. 1-4). Of prime interest to the NASA Lewis H_2-O_2 MHD program is the development of lightweight, multi-megawatt MHD power supplies. The major difficulty in their development is their small size which makes surface losses (thermal and electrical) a significant fraction of the power generated. To overcome these losses, these generators must be operated at high Mach numbers and high magnetic field. Therefore, our initial experimental program is directed toward evaluating the performance of H_2-O_2 generators at high voltage, i.e., high Mach number (2), and high magnetic field (7 Tesla).

Two facilities are being used in the NASA Lewis H_2-O_2 experimental program. The primary facility is the MHD power generation facility which was previously described in reference 1. The main feature of this facility is a liquid neon-cooled cryomagnet capable of a 7 Tesla peak field. At present, construction of this facility has been completed and systems checkout is in progress.

The second facility is a rocket test facility for testing MHD hardware and performing diagnostic tests on the alkali-metal seeded combustion plasma and MHD duct. This facility has no magnet and, therefore, diagnostic measurements are made with applied electric fields. This facility is shown in operation in figure 1. Shown are the injector-combustion chamber-nozzle and a prototype MHD Hall generator. At present, over 1000 test runs for times ranging from a few seconds to 20 seconds have been performed in this facility. These tests were performed to develop interelectrode insulating materials, to measure heat losses, and to measure the fluid dynamic and electrical properties of MHD ducts and the cesium seeded H_2-O_2 working fluid.

II. Combustion Chamber-Nozzle Heat Loss Tests

An initial concern with the water-cooled copper combustion chambers (including supersonic nozzle) was that these chambers were designed to operated steady state with wall temperatures somewhat beyond the boiling point of water, but considerably below the condensation point for CSOH. These chambers therefore have two undesirable features due to the low wall temperature: possible high heat loss and condensation of CSOH which could then short out the MHD channel by streaming down the channel as a liquid. To alleviate these problems, a second set of combustion chamber-nozzles was constructed with a 0.006-inch graded mixture of zirconia/nichrome flame sprayed on their inner surface. This provides an allowable surface temperature well above the condensation temperature of CSOH.

The net heat loss from these two designs was determined by measuring the cooling water flow rate and temperature difference from inlet to outlet. The measured values are shown in figure 2 as a function of combustion chamber pressure. Surprisingly the heat transfer to the hot wall ceramic-coated chambers is higher than to the cold wall copper chambers. Optical pyrometer measurements in the supersonic portion of the combustion chamber-nozzle verified that the ceramic coating did produce a surface temperature of approximately 1500° K in this region.

To gain some understanding of these results, a simplified heat transfer calculation based upon unaccelerated flows was carried out. This simplification leads to an overestimate of the heat flux in the accelerating-deaccelerating region around the throat of the nozzle. However, since the surface area of this region is relatively small compared to that of the total surface area of the combustion chamber-nozzle, the effect upon the net heat transfer should be small. (For a discussion of this point see ref. 5.) If one assumes fully turbulent flow throughout the combustion chamber-nozzle, the heat flux, q, is given by

$$q = 0.026 \frac{k}{D} (Re)^{0.8} (Pr)^{0.3} (T_{ad} - T_w) \qquad (1)$$

where: k is the thermal conductivity
D is the duct diameter at the point at which the heat flux is evaluated
Re is the Reynolds number
Pr is the Prandtl number
T_{ad} is the adiabatic temperature

$$\equiv T + (Pr)^{1/3}(T_s - T) \qquad (2)$$

T is the static temperature of the flowing gas
T_s is the stagnation temperature of the flowing gas
T_w is the combustor-nozzle wall temperature

and k, Re, and Pr are evaluated at the reference temperature condition,

$$T_r = T + 0.5(T_w - T) + 0.22(T_{ad} - T) \qquad (3)$$

The above equations are those of reference 5 for unaccelerated flows except they are for a heat transfer coefficient based upon temperature rather than enthalpy. This was done so that tabular data from reference 6 could be used to evaluate viscosity, thermal conductivity, and heat capacity. These coefficients were evaluated assuming chemical equilibrium through the boundary layer.

The heat flux from the gas (eq. (1)) is then equal to the heat flux through the chamber wall given by

$$q = \frac{T_w - T_l}{\left(\frac{\Delta x}{K}\right)_{coat} + \left(\frac{\Delta x}{K}\right)_{cu} + \frac{1}{h_l}} \qquad (4)$$

where: T_l is the temperature of the cooling water
$\left(\frac{\Delta x}{K}\right)_{coat}$ and $\left(\frac{\Delta x}{K}\right)_{cu}$ are the thickness/thermal conductivity for the ceramic coating and copper wall, respectively

h_l is the film coefficient for the cooling water

The properties of the flowing gas are determined by integrating the pressure and temperature equations for the flowing gas through the contour of the combustion chamber-nozzle. These equations include heat transfer (eq. (1)), friction (smooth pipe) and equilibrium chemistry (ref. 7). The problem of the singular point at Mach = 1 is removed by integrating subsonically until (1 - Mach) $\leq$ 0.001 and then jumping across to Mach =1.001. The integration technique is Runge-Kutta-Merson (ref. 8) whose variable step size allows the treatment of the singularity to be programmed into the logic.

The heat transfer at each station of the integration is determined by iteratively solving equations (1) to (4) for the unknown temperatures T_{ad}, T_w, T_r, and the heat flux q. Note that T and T_s are given by the gas dynamic calculation and cooling water temperature T_l is taken to be room temperature.

The results of this calculation are shown by the solid lines in figure 2. The agreement with experiment is good and indeed the theory predicts that the total heat transfer to the hot wall ceramic coated combustors is greater than that to the cold wall copper combustors. Examination of the results of the theoretical calculations indicated that the reason for this apparent anomaly is that while the factor $T_{ad} - T_w$ (eq. (1)) decreases with increasing wall temperature, i.e., for the ceramic coating, this decrease is more than offset by the increase in the thermal conductivity resulting from the increase in T_r (eq. (3)).

III. Fluid Dynamic Tests

Another concern was with the fluid dynamic performance of the nozzle. The design was adapted from a previous rocket program and involved a compromise between achieving a low weight and perfectly parallel flow. Careful pressure probing at 0.635 cm (0.25 in.) intervals from the end of the nozzle to a point approximately 8 cm downstream indicated the presence of a pressure disturbance approximately 5 cm downstream of the nozzle exit. The data are shown in figure 3. The symbols on the figure correspond to the following channel configurations.

1. □ 12-0.635 cm (0.25 in.) electrodes with pressure taps on electrodes 1, 3, 5, 7, 9, and 11 as numbered from the nozzle

2. × 2.54 cm (1 in.) spacer between nozzle and the above channel

3. ◇ channel as in 1 except turned end for end

4. + 30-0.127 cm (0.5 in.) electrodes with 2.54 cm spacer between nozzle and channel with pressure taps on all but electrodes 10, 11, and 20

To understand the nature of this disturbance, the experimental conditions were analyzed using a three-dimensional supersonic nozzle analysis (ref. 9). This is a modification of the scheme of reference 10 which is an exact solution to the characteristic equations and is accurate to second order in the grid spacing. While the analysis smooths out the sharp changes across a shock wave and ignores all dissipative effects, reference 9 shows that it predicts the location and magnitude of strong compressions fairly well. The theoretical prediction (shown in fig. 3) is seen to agree well with the experimental data as to the location and magnitude of the first oblique shock. Some recent data taken in a MHD duct built for initial tests in our magnet facility are also shown by the crossed points in figure 3. While the data are of insufficient resolution to establish the exact structure of the downstream pressure disturbances, there is evidence of at least quantitative agreement with theory.

Also shown on figure 3 is a one-dimensional MHD channel calculation including friction, heat transfer, and chemistry. This calculation is similar to that described in the previous section with the exception that in keeping with the results observed by others (ref. 11 and references included therein), the skin friction coefficient was increased by a factor of 3 over the smooth wall value to compensate for the rough wall structure of the segmented MHD duct. Again, the agreement is good. Note that the agreement is not with an average through the data since the distance over which the shocks occur is small compared to the distance between shocks. Therefore, the theory should be more heavily weighted by the points in the valley rather than the peaks of the pressure disturbance (compare 1-D isentropic and 3-D nondissipative).

While the observed pressure disturbances do not appear to cause additional pressure drop over that resulting from rough walls, their effect upon the performance of the duct in the presence of a magnetic field is open to question. The pressure disturbances can lead to nonuniformities in the electrical conductivity and/or Hall parameter which in turn may lead to a deterioration in performance of the generator in the presence of a magnetic field. Such deterioration has been predicted theoretically for plane, layered nonuniformities in these parameters (see ref. 11 and references cited therein).

IV. Electrical Conductivity Tests

Electrical conductivity tests were performed in constant area, heat sink, cylindrical, Hall type MHD channels. The electrical conductivity was measured in the classical manner (see ref. 12) by applying a voltage across the channel from one end electrode to the other, measuring the current, and using the inner electrodes as probes to monitor the voltage distribution along the channel. Typical voltage profiles are shown in figure 4 as a function of time. The channel used in this test consisted of 12-1.27 cm (0.5 in.) wide electrodes separated by synthetic mica insulators. It is noted from this figure that there are voltage drops at both ends of the channel with a linear region in the central portion. The voltage drops are associated with the current flow across the cold boundary layer and then into the larger area associated with uniform current flow through the channel. Therefore the linear region is representative of the electrical properties of the gas and hence was used to infer the average electrical conductivity of the gas from

$$\sigma = \frac{I}{A(\Delta V/\Delta X)}$$

where: σ is the electrical conductivity
A is the cross sectional area of the channel
$\Delta V/\Delta X$ is the voltage gradient determined from the voltage curves
I is the measured current

For the test data shown in figure 4, the working fluid was a stoichiometric mixture of H_2-O_2 at a combustion pressure of 1.034×10^6 N/M^2 (150 psia). The Mach 2 flow was seeded with a 75% solution of CSOH dissolved in water. The solution was sprayed into the oxygen feed line. For this test the following data were obtained.

Time (sec)	σ(MHO/M)	I (Amp)	$\Delta V/\Delta X$ (volts/M)
2.08	12.62	1.762	72.4
3.08	13.16	2.037	80.3
4.08	12.89	2.112	85.0

where $\Delta V/\Delta X$ is the value in the linear region (electrodes 3-8).

It is noted that the value of the gas conductivity does not change appreciably during the run. However, the measured current varies from 1.762 to 2.112 amps due to the increase in $\Delta V/\Delta X$. This is a result of the decrease in the electrode voltage drop at the ends of the channel. This decrease in voltage drop is the result of the increasing wall temperature of the heat sink channel with run time and the consequent increased temperature of the boundary layer.

In figure 5 the results of several conductivity measurements are given. The solid curves are theoretical values calculated using the chemistry of reference 7 to calculate the free electron density taking into account a 3% heat loss in the combustor-nozzle and a 1% heat loss in the channel. The calculated values are the local values at the midpoint of the channel. The only important contributions to the collision frequency are from H_2O and cesium compounds. The H_2O cross section was taken from reference 13. Cesium and its compounds were given the cross section from reference 14. Cross section values were assigned to all other species, but due to their unimportance and number (31) they will not be referenced.

The seed fractions over which conductivity data has so far been taken is limited by the size of the seed flow meter. Therefore as noted in figure 5, the range changes as we increase the combustion pressure, i.e., H_2-O_2 mass flow. However, the following conclusions can be drawn. For a combustion pressure of 2.069×10^6 N/M^2 (300 psia) the experimental data are in good agreement with theory. At a combustion pressure of 1.034×10^6 N/M^2 (150 psia) the experimental data agree with theory up to a seed fraction of approximately 0.05 at which point it decreases well before the expected maximum at a seed fraction of 0.15. The experimental points at a combustion pressure of 5.17×10^5 (75 psia) are nearly a factor of 5 below theory and show no dependence on seed fraction.

The lower than predicted electrical conductivity at higher seed fractions and/or lower pressures is thought to be due to poor atomization of the seed as the ratio of seed mass flow/oxygen mass flow increases. This effect is well known from studies of two-fluid atomization, e.g., reference 14, where it is shown that the droplet size increases rapidly as the ratio of liquid to gas mass flow increases. In our experiment these larger droplets may be of sufficient size that they are not vaporized during their residence time in the combustor. This effect would be increasingly noticeable at lower pressures as is observed in our experiments.

V. Concluding Remarks

This study has shown that flame sprayed ceramic coatings on combustion chamber and nozzle walls permits operation with hot walls, thereby eliminating possible problems associated with seed condensation. However, under the conditions of our experiment the net heat transfer was unexpectedly increased over that of cold copper walls. Further work will be concerned with comparing the electrical conductivity of the gas at the exit of these nozzles.

Pressure disturbances associated with oblique pressure waves have been measured in our MHD channel. These disturbances are due to a rocket-type nozzle which was designed to achieve low weight rather than perfectly parallel flow at the exit. A new nozzle with parallel flow at the exit has been designed and will be used in our magnet facility along with the previous nozzles to study the effect of the pressure disturbances upon the performance of the MHD generator.

Electrical conductivity measurements were found to be in good agreement with theory except at low combustion pressures and/or high ratios of seed/oxygen mass flows (seed was injected into oxygen flow line). The discrepancy is believed to be the result of poor atomization of the seed at high ratios of seed/oxygen mass flows which results in droplet sizes which do not completely vaporize during their residence time in the combustor. This problem is being analyzed spectrographically.

VI. References

1. Smith, J. M.; Nichols, L. D.; Seikel, G. R.: NASA Lewis H_2-O_2 MHD Program. 14th Symp. on the Engineering Aspects of Magnetohydrodynamics. Univ. Mississippi Press, 1974, pp. III.7.1-III.7.5.

2. Stangeby, P. C.: Comparative Economics for H_2-O_2 MHD Emergency and Peaking Power Production. Sixteenth International Conference on Magnetohydrodynamic Electrical Power Production. Vol. 4, Intl. Atomic Energy Agency, 1975, pp. 9-21.

3. Nakamura, T.: Feasibility of H_2-O_2 Closed Cycle MHD Power Generation Based upon Thermochemical Decomposition of Water. Sixth International Conference on Magnetohydrodynamic Electrical Power Production. Vol. 4, Intl. Atomic Energy Agency, 1975, pp. 39-52.

4. Townsend, S. J.: The Economic Implications of the CANCO H_2/O_2 MHD Energy Storage System Used as an Intermediate Load and a Peaking Generator. Sixth International Conference on Magnetohydrodynamic Electrical Power Production. Vol. 5, Intl. Atomic Energy Agency, 1975, pp. 169-179.

5. Boldman, Donald R.; Graham, Robert W.: Heat Transfer and Boundary Laye~ in Conical Nozzles. NASA TN D-6594, 1972.

6. Svehla, R. A.: Thermodynamic and Transport Properties for the Hydrogen-Oxygen System. NASA SP-3011, 1964.

7. Gordon, Sanford; McBride, Bonnie J.: Computer Program for Calculation of Complex Chemical Equilibrium Compositions, Rocket Performance, Incident and Reflected Shocks, and Chapman-Jouquet Detonations. NASA SP-273, 1971.

8. Merson, R. H.: An Operational Method for the Study of Integration Processes. Proc. Symp. on Data Processing. Weapons Research Establishment, Salisbury (Australia), 1957, p. 24.

9. Bishop, Allan R.; Sanders, Bobby W.: Modification of a Three-Dimensional Supersonic Nozzle Analysis and Comparison with Experimental Data. NASA TM X-3025, 1974.

10. Ransom, Victor H.; et al.: A Second Order Numerical Method of Characteristics for Three-Dimensional Supersonic Flow. Volume 2: Computer Program User's Manual. Purdue Univ. (AD-865803;AFAPL-TR-69-68-Vol.-2), 1970.

11. Nichols, L.D.: Effective Electrical Conductivity of a Nonuniform Plasma. Phys. Fluids, vol. 18, no. 7, July 1975, pp. 920-921.

12. Heywood, J. B.; and Womack, G. J., eds.: Open Cycle MHD Power Generation. Pergamon Press (London), 1969, p. 346.

13. Kuhne, W. D.; and Kolb, G.: Angewandt Magnetohydrodynamik-Heft 9. Berechnung der Kenngrossen von Arbeitsgasen des MHD-Verbrennungsgas-Generators. (Applied Magnetohydrodynamics. Volume 9 - Calculation of the Characteristic Quantity of the Working Gas of the MHD-Combustion Gas Generator). Jul-874-TP, Institut Fuer Technische Physik, Juelich (West Germany), 1972.

14. Heighway, John E.; and Nichols, Lester D.: Brayton Cycle Magnetohydrodynamic Power Generation with Nonequilibrium Conductivity. NASA TN D-2651, 1965.

15. Kim, K. Y.; Marshall, W. R., Jr.: Drop-Size Distributions from Pneumatic Atomizers. Am. Inst. Chem. Engrs. J., vol. 17, no. 3, May 1971, pp. 575-584.

E-8675

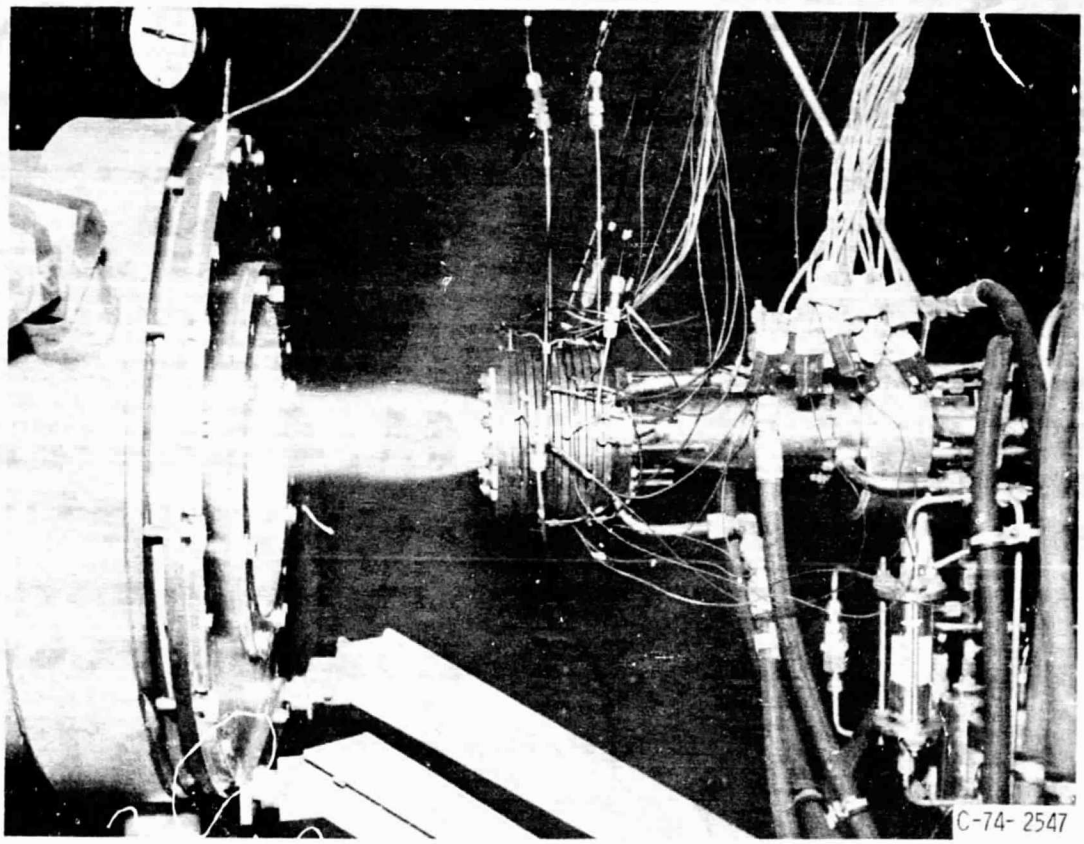

Figure 1. - Rocket Lab test facility.

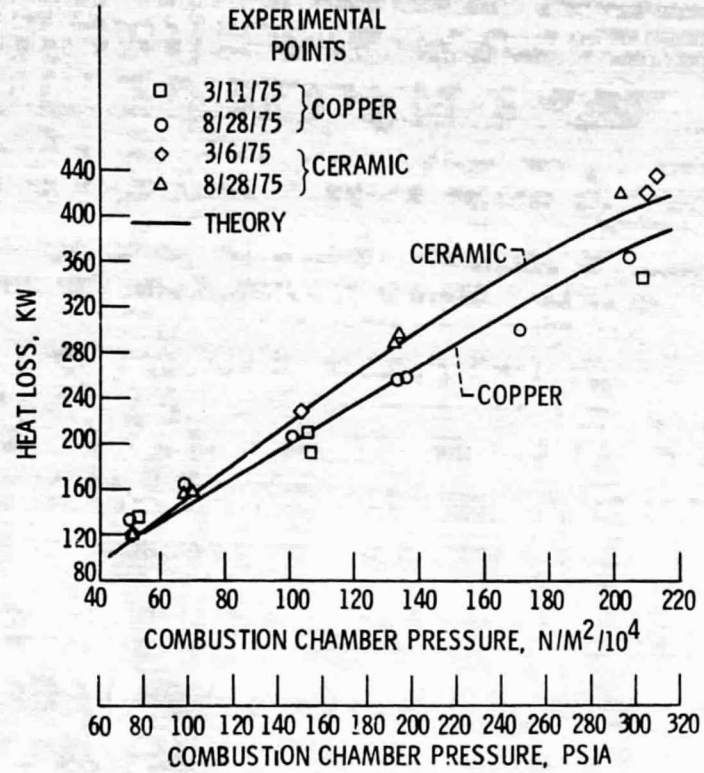

Figure 2. - Combustor-nozzle heat loss versus combustion pressure.

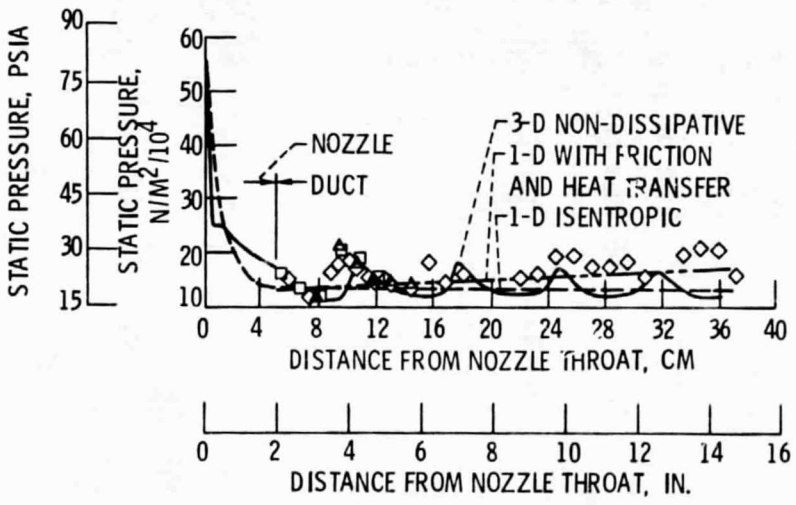

Figure 3. - Static pressure distribution along supersonic nozzle section and channel.

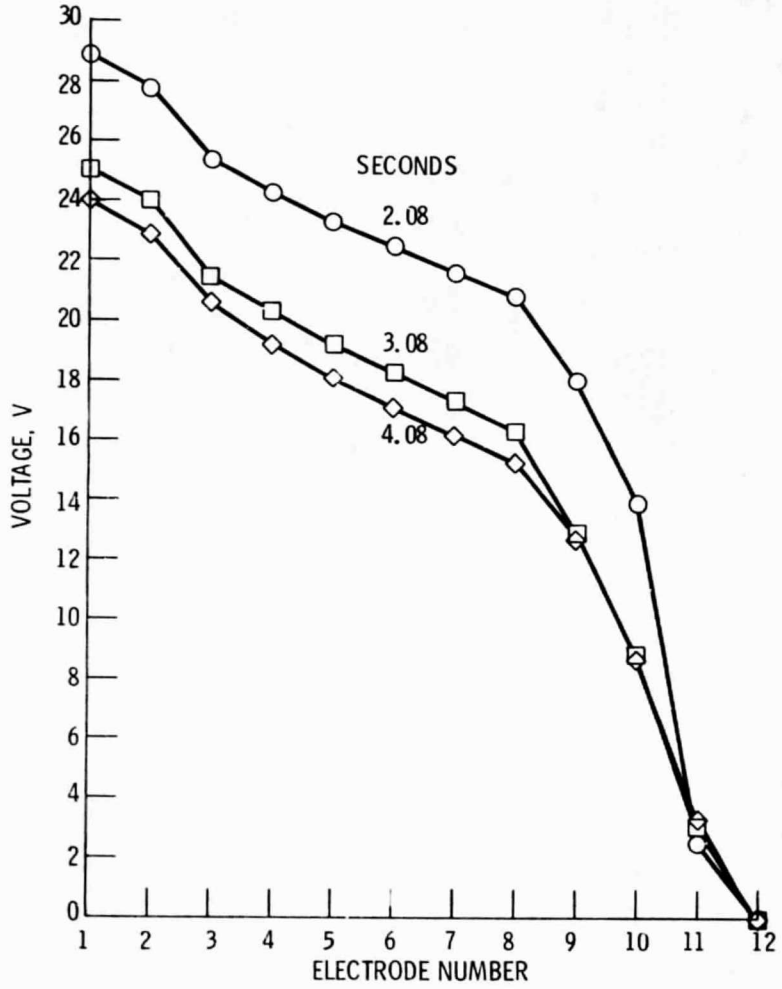

Figure 4. - Voltage distribution along channel as function of run time.

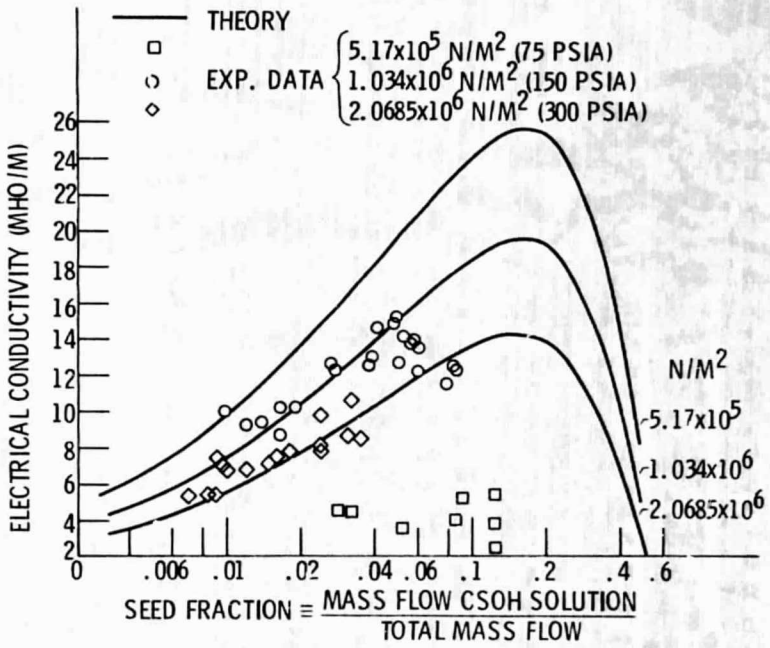

Figure 5. - Electrical conductivity versus seed fraction as a function of combustion pressure

NASA-Lewis